# Demonstration of 30 GHz OIP3/PDC > 10 dB by mm-wave N-polar Deep Recess MISHEMTs

Matthew Guidry, Brian Romanczyk, Haoran Li, Elaheh Ahmadi, Steven Wienecke, Xun Zheng, Stacia Keller, and Umesh K. Mishra
Department of Electrical and Computer Engineering, University of California
Santa Barbara, CA 93106
Email: mguidry@ece.ucsb.edu

***Abstract*—Nitrogen-polar gallium nitride deep recess high electron mobility transistors have recently demonstrated exceptional mm-wave power density and efficiency when measured at 30 and 94 GHz. In addition to power and efficiency, linear operation with low DC power consumption is important because nonlinearities generate distortion and interference in both transmitters and receivers. This work presents the first measurements and analysis of the OIP3 and OIP3/$P_{DC}$ for an N-polar GaN deep recess device. An OIP3/$P_{DC}$ of up to 11.4 dB is demonstrated at 30 GHz using a vector receiver load pull system, and the linearity studied as a function of the bias current density.**

***Keywords—Gallium Nitride; GaN; HEMT; MISHEMT; linearity; OIP3; efficiency; Ka-band; mm-wave; N-polar; power amplifier; low noise amplifier; Load pull;***

## I. Introduction

Gallium Nitride (GaN), with its high critical electric field, mobility, and saturation velocity has established itself as a leading material for mm-wave power amplifiers (PAs) [1]. Wireless link range and data rate is a function of the link budget in terms of transmitter power and receiver noise figure. The high power and efficiency enabled by GaN at RF and mm-wave frequencies has led GaN to be increasingly adopted for power amplifiers in wireless systems. Its capability for high gain with high breakdown voltage has also led to its application in high reliability receiver low noise amplifier (LNA) applications [2]. High performance switches are also enabled [3], thus allowing GaN to cover a full range of transceiver front-end components with high performance.

N-polar GaN deep recess MISHEMTs in recent years have demonstrated record device-level CW power performance at mm-wave frequencies. Romanczyk *et al.* [4] reported a constant 8 W/mm power density measured from a single device by load pull at 10, 30, and 94 GHz, with corresponding record or near-record power added efficiencies (PAE). Many of the reasons for this excellent performance are discussed in [1], [4], [5]. A large portion of the performance advantage is attributed to the *in-situ* grown GaN cap which serves a dual purpose of providing excellent dispersion control and enhancing conductivity of the access regions.

In the increasingly crowded wireless spectrum, interference caused by nonlinear distortion has a large influence on spectrum planning and the performance of wireless links [6]. This places greater emphasis on the linearity of circuits and the underlying semiconductor devices. Distortion in a power amplifier causes the power of a modulated signal to be spread out of the intended frequency band and into adjacent bands where it can interfere with other receivers. Distortion in receiver components can allow large out-of-band signals to produce interference inside receiver passbands.

Because of this, understanding and improving the linearity of semiconductor devices is of great relevance. This linearity is often quantified through a measurement of the output third order intercept power (OIP3) [6]. In general the OIP3 can be improved by any factor by an increase in the DC power consumption ($P_{DC}$) of nearly the same factor. A trivial example of this would be combining multiple copies of an amplifier in parallel using power division and combination. Therefore the ratio of these numbers, OIP3/$P_{DC}$ is the best metric for comparing linearity between devices. N-polar GaN planar MISHEMT devices have already shown promising results. Arias *et al.* [7] have reported on a 12 dB ratio of OIP3/$P_{DC}$ at 10 GHz and up to 8.4 dB at 30 GHz [8]. This work reports for the first time on the device-level linearity of deep recess N-polar GaN MISHEMTs at 30 GHz.

## II. Device and Experimental Details

### A. Device Structure

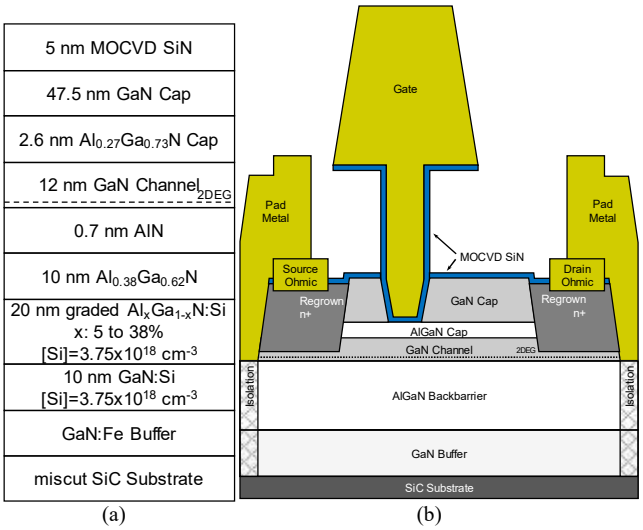


**Fig. 1.** (a) Epitaxial structure and (b) cross-section (not to scale) of the N-polar GaN deep recess MISHEMT, from [9].

The device is designed to provide high gain and power density at mm-wave frequencies, including 94 GHz. The schematics of the epitaxial layer and device structures are shown in Fig. 1. The details of the design and fabrication of this device are described more fully in [4], and will not be discussed in detail here. The GaN cap, because of the direction of polarization fields in N-polar GaN, enhances both the channel charge density [10] and mobility [11]. This leads to reduced on-resistance and increased maximum current which improves the power density at a given drain bias. The high quality *in-situ* interface to the underlying epi and low bulk trap density inherent to a high quality semiconductor helps provide excellent dispersion control.

All device measurements were performed on wafer with the full thickness SiC substrate and CPW probe pads for a device with a gate width of 2 x 37.5 µm, 75 nm gate length, 75 nm gate-to-source spacing, and 400 nm source to drain spacing.

### *B. Two-Tone Vector Receiver 30 GHz Load Pull Measurement*

The 30 GHz OIP3 measurements were performed with a vector receiver load pull (VRLP) system at Maury Microwave. A diagram of the system is shown in Fig. 2. The vector network analyzer (VNA), a Keysight PNA-X, is used heavily for the measurement: It supplies the two tones centered around 30 GHz from a single test port using its two internal sources and combiners. External couplers are connected close to the GSG wafer probes to sample the forward and reverse a- and b-waves using the VNA's vector receivers. This setup bypasses the internal couplers of the VNA to provide a high directivity close to the device under test (DUT) reference plane. The VNA has a low noise floor and high dynamic range in order to measure the IM product power levels at low input powers as well as the fundamental tones at much higher power levels.

In the VRLP configuration a source-side tuner is not necessary and was not used here because the DUT's complex input reflection coefficient ($\Gamma_{in}$) and the delivered input power ($P_{in,delivered}$) are measured, allowing determination of the operating power gain ($G_P$). Source pull contours can be determined mathematically from this data [12]. The drawback of not using a source tuner is that the system PA must have sufficient drive power available to overcome the large mismatch at the input of the device. A PA with a 9 W $P_{Sat}$ was used here.

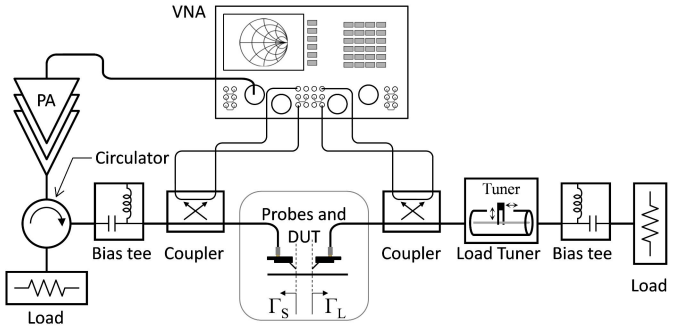


**Fig. 2.** Schematic of vector receiver load pull system used in this work.

A tone spacing of 10 MHz was used for the measurements presented here. The tone spacing should not be too large in a passive load pull system. With the physical tuner spaced by a non-zero phase delay away from the DUT, this leads to a difference in the actual load reflection coefficient ($\Gamma_L$) at the DUT's output plane for the fundamental tones and their IM products. Active load pull can overcome this and provide a controlled $\Gamma_L$ at the input tones and their IM products, or even across the bandwidth of a more complex modulated signal [13], though commercially available active load pull configurations typically have a higher noise floor than the VRLP system configured here.

### *C. Bias point selection based on DC linearity analysis*

The nonlinearity of the transistor's DC drain current was used to guide the measurement plan for this work based on a simplified analysis, to capture bias conditions of interest with higher and lower values of OIP3 and OIP3/$P_{DC}$. While several aspects of the device contribute to distortion, the transconductance ($g_m$) nonlinearity tends to be the most dominant effect in producing distortion [14]. Effects which were neglected here are the dependence of $I_{DS}$ on $V_{DS}$, nonlinearity of source resistance [15], charge storage nonlinearity (capacitances), and memory effects including dispersion and self-heating. With these simplifications a power series analysis can be used for small signal levels, instead of a Volterra series [14].

The small signal output current at low input powers is treated as a third order Taylor series (1), with coefficients as in (2). From the Taylor series the OIP3 in dBm can be calculated in (3), where $R_L$ is the load resistance [6]. It is noted that $g_{m1}$ is the typical definition of transconductance; if $g_{m1}$ were perfectly flat then the higher order derivatives including $g_{m2}$ and beyond would be zero, and neglecting other sources of distortion, OIP3 would be infinite.

$$i_{ds}(v_{gs}) = g_{m1}v_{gs} + g_{m2}v_{gs}^2 + g_{m3}v_{gs}^3 \tag{1}$$

$$g_{m1} = \frac{dI_{DS}}{dV_{GS}};\ g_{m2} = \frac{1}{2}\frac{d^2I_{DS}}{dV_{GS}^2};\ g_{m3} = \frac{1}{6}\frac{d^3I_{DS}}{dV_{GS}^3} \tag{2}$$

$$OIP3\ (\text{dBm}) = 10\log_{10}\left(\frac{2}{3}\frac{g_{m1}^3}{g_{m3}}R_L\right) + 30 \tag{3}$$

The drain source current as a function of gate-source voltage ($I_{DS}(V_{GS})$) was measured at $V_{DS}$ of 10 V using a parameter analyzer. This measured data contains noise and successive numeric differentiation amplifies that noise. This causes $g_{m2}$ and $g_{m3}$ to typically be very noisy based on direct numeric differentiation of the measured data. Data smoothing using a simple nonlinear Angelov-based model [16] was used to obtain smooth derivatives. The measured data and corresponding model fit are shown in Fig. 3 (a) which shows good fit for both linear and log scales. The derivatives were then calculated as in (2), based on this model, and are shown in Fig. 3 (b). Eqn. (3) was then used with $g_{m1}$ and $g_{m3}$ to predict the OIP3 and OIP3/$P_{DC}$. As is typically seen there is a zero

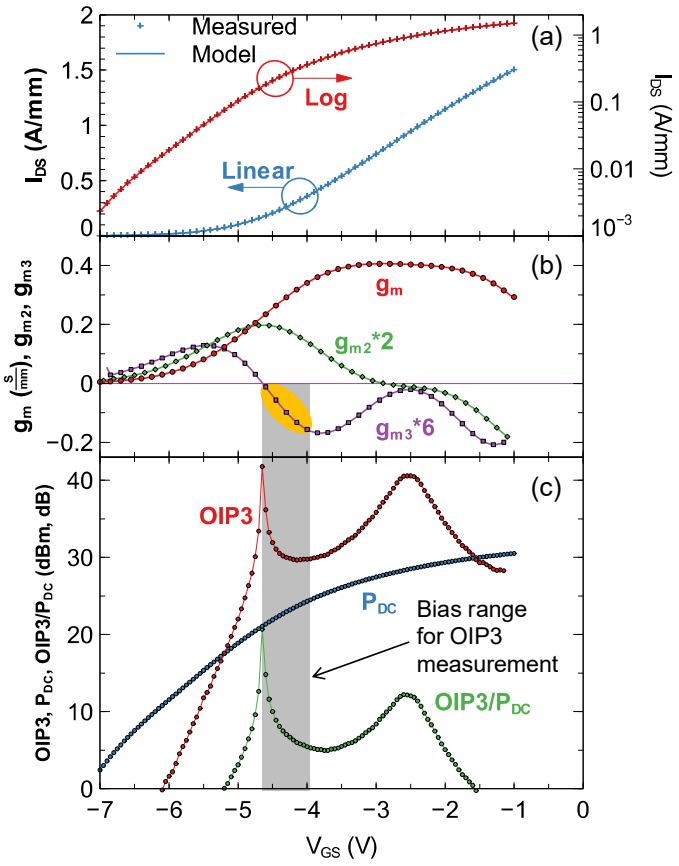


**Fig. 3.** (a) DC $I_{DS}(V_{DS})$ with the data in markers and smooth model fit with solid lines of deep recess device at $V_{DS}$=10 V, (b) Extracted derivatives of $I_{DS}(V_{GS})$ from model. $g_{m2}$ and $g_{m3}$ are scaled for greater visbility. (c) The DC power consumption ($P_{DC}$) and the predicted OIP3 and OIP3/$P_{DC}$ ratio as a function of $V_{GS}$. The bias range selected for OIP3 measurement is highlighted in (b) and (c).

crossing of $g_{m3}$ during the initial turn-on of the device, where the $g_{m1}$ is rising the fastest, with a corresponding narrow peak in OIP3 and OIP3/$P_{DC}$. This narrow peak is not practical to use in a circuit because of the sensitivity of the peak location to process or temperature variation, and it would only apply for very small signal levels. But the region from this zero crossing to the first negative $g_{m3}$ minimum was selected as the bias range for this OIP3 measurement, as this is expected to show a range of OIP3/$P_{DC}$ results, from a high peak above 10 dB to a low value of about 5 dB. The gate bias for this range includes -4.7 V to -3.8 V, with corresponding current density of 170 to 430 mA/mm and is highlighted in Fig. 3 (b), (c).

## III. Results

Large signal, 30 GHz two-tone load pull measurements were taken with the drain voltage at 10 V and the quiescent drain-source current ($I_{DSQ}$) varied from 161 to 500 mA/mm in a total of five steps. This covers the bias range selected as described section II.C to investigate the varying effects of DC power as well as the varying transconductance and higher derivatives ( $g_{m1}$, $g_{m3}$ ). Of these bias conditions, two of specific interest are plotted in detail to highlight in Fig. 4. The plots contain, as a function of swept input power, the total output power of the fundamental tones as well as the absolute power of the upper (Hi) and lower (Lo) intermodulation products ($P_{I3}$), OIP3, OIP3/$P_{DC}$, power gain ($G_P$), and PAE.

In Fig. 4 (a) the device is biased at 292 mA/mm, which is a moderate class AB bias, near 20% of $I_{DS,max}$. The slope of $P_{I3}$ is close to 3:1, which is to be expected as third order effects tend to dominate at these lower power levels. The device exhibits an excellent OIP3/$P_{DC}$ above 10 dBm at input powers below 0 dBm, with OIP3 above 34 dBm. The 0 dBm input power also corresponds to 10 dB of input power back-off from the 1 dB gain compression point ($P_{1dB}$). As the input power is dropped much further below 0 dBm the data becomes noisy due to the absolute power levels approaching the noise floor of the receivers. This becomes especially apparent for $P_{I3}$ power levels at the DUT output below -60 dBm, which corresponds to -75 dBm at the VNA receivers, incorporating an estimated total loss of 15 dB for the coupling factor and interconnects.

Fig. 4 (b) shows the operation at a deeper class AB bias of 161 mA/mm. For $P_{in}$ below 0 dBm the device shows the classic 3:1 slope of $P_{I3}$ versus $P_{in}$. At higher power levels beginning near 0 dBm of input power, $P_{I3}$ exhibits a pronounced sweet spot [17] in OIP3. This leads to a localized peak in the OIP3/$P_{DC}$ ratio. This is likely because at the lower bias current density and high drive power the device $V_{GS}$ reaches the more strongly nonlinear turn-on regime at a lower input power. Beyond the sweep spot the $P_{I3}$ tones have close to a 5:1 slope as higher order effects dominate, which is not captured in the third-order power series analysis used to guide this measurement.

A comparison of OIP3, $P_{DC}$, and OIP3/ $P_{DC}$ over all measured current densities is shown in Fig. 5. For this plot, data approaching or below the noise floor was removed for clarity. This comparison as a function of input power also includes some of the effect of varying gain levels. In order to better compare results at similar normalized drive levels, the results are summarized in Fig. 6 and TABLE I. at two back-off levels from the 1 dB gain compression point ($P_{1dB}$) to highlight differences between the weakly and more strongly nonlinear regions of operation. 15 dB back-off is in the weakly nonlinear regime for all bias conditions, where slopes of $P_{I3}$ are near 3:1. 10 dB back-off is in the more strongly nonlinear regime which can show higher order effects including sweet spots.

The 15 dB back-off summary in Fig. 6 and TABLE I. show that OIP3/$P_{DC}$ peaked at 11.4 dB at a bias of -4.3 V and 292 mA/mm. A peak in OIP3/$P_{DC}$ appears to be centered at 270 mA/mm. At current densities above this peak the OIP3/$P_{DC}$ decreased as expected and reached a low value of 5.8 dB at 500 mA/mm bias current. The trend of the peaked response and values are relatively consistent with the predictions based on the $I_{DS}(V_{GS})$ analysis, though the measured bias current of the peak OIP3/$P_{DC}$ was offset slightly from the predicted location.

The 10 dB back-off summary in Fig. 6 and TABLE I. show OIP3/$P_{DC}$ monotonically improving over this range as $I_{DSQ}$ is reduced. This is due to a combination of factors including the sweet spot formation at deeper class AB bias, reduced $P_{DC}$ at lower $I_{DSQ}$, and the relative values of $g_{m1}$ and $g_{m3}$ as a function of $I_{DSQ}$.

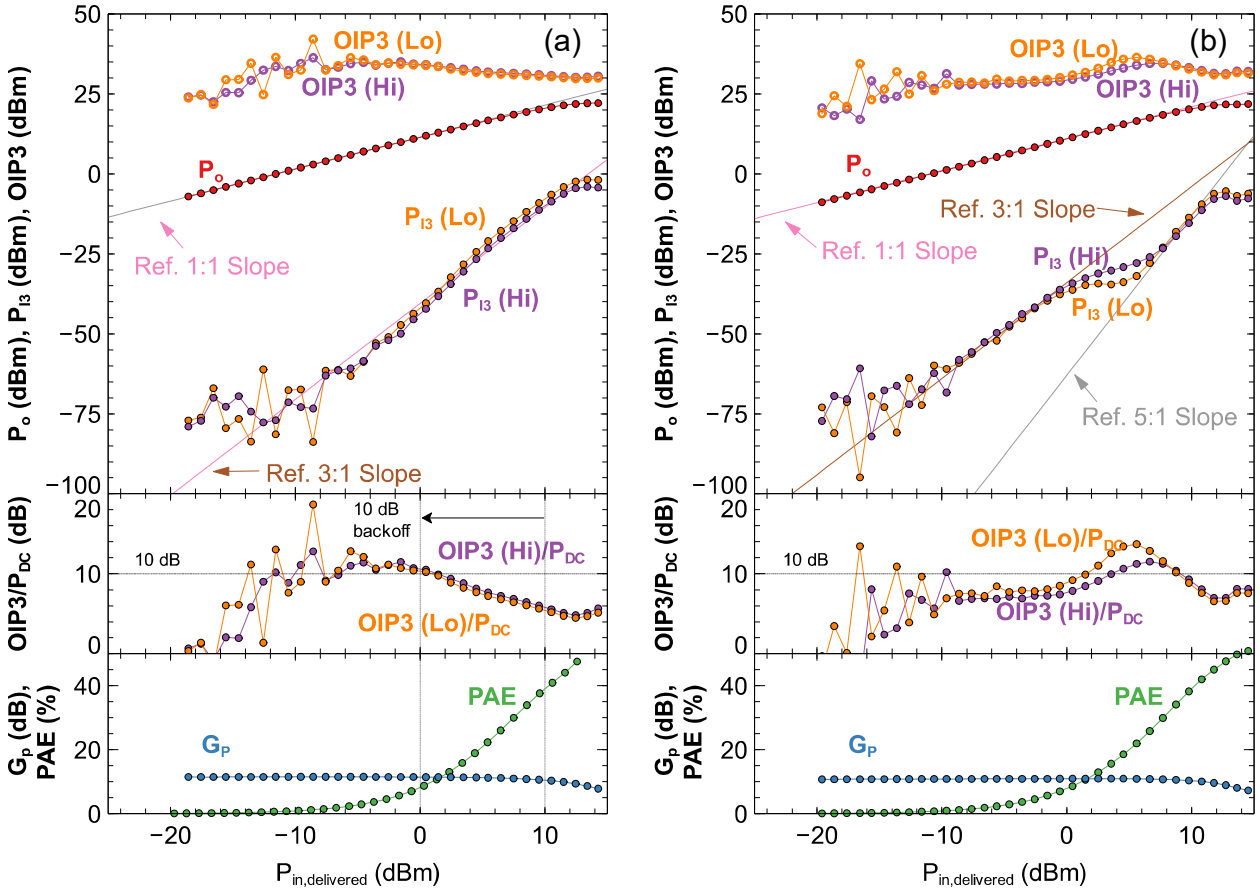


**Fig. 4.** Two-tone power sweep at $V_{DS}$=10 V and $I_{DSQ}$ of (a) 292 mA/mm, showing > 10dB OIP3/PDC at 10 dB back-off from P1dB, and (b) 161 mA/mm exhibiting a sweet spot with higher OIP3/PDC, and a 5:1 slope thereafter. Both the upper (Hi) and lower (Lo) IM products and their corresponding OIP3 and OIP3/$P_{DC}$ are shown.

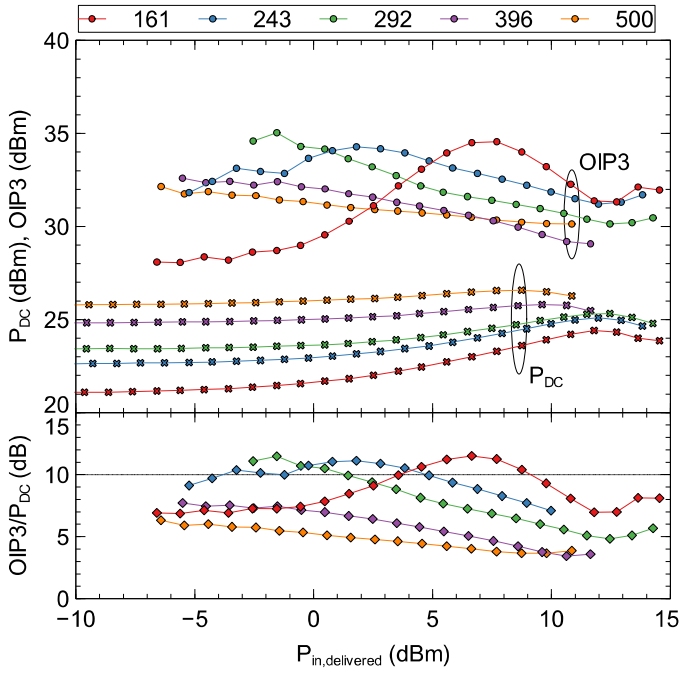


**Fig. 5.** Summary of OIP3 (Hi), $P_{DC}$, and OIP (Hi)/$P_{DC}$ as a function of input power for every bias condition.

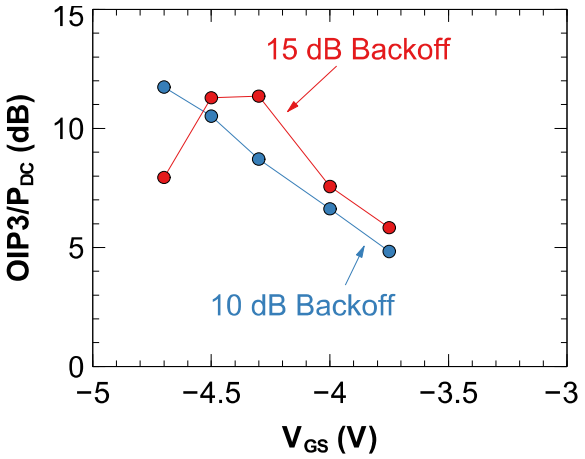


**Fig. 6.** Summary of OIP3/$P_{DC}$ as a function of $V_{GS}$.

TABLE I. MEASUREMENT SUMMARY

| $V_{GSQ}$ (V) | $I_{DSQ}$ (mA/mm) | OIP3/$P_{DC}$ (dB) at 10 dB backoff | OIP3/$P_{DC}$ (dB) at 15 dB backoff |
|---|---|---|---|
| -4.7 | 161 | 11.7 | 7.9 |
| -4.5 | 243 | 10.5 | 11.3 |
| -4.3 | 292 | 8.7 | 11.4 |
| -4.0 | 396 | 6.6 | 7.6 |
| -3.75 | 500 | 4.8 | 5.8 |

## IV. Conclusions

This first report on the linearity of N-polar GaN MISHEMTs using VRLP measurements, where they exhibited OIP3/$P_{DC}$ values up to 11.4 dB at 30 GHz and a $V_{DS}$ of 10 V. A study of the OIP3/$P_{DC}$ as a function of the bias current density was carried out based on a simplified device model. This study showed that the device exhibits a peaked response in OIP3/ $P_{DC}$ , with the location of the peak and the values observed being reasonably consistent with the model at low input powers where the device exhibits weakly non-linear behavior. The device also exhibited localized sweep spots with higher OIP3/$P_{DC}$ due to higher order effects which were not represented by the model. Future work will investigate more advanced models to better understand and predict distortion, and modifications to the device for higher linearity performance with low power consumption.

## Acknowledgment

The authors thank Teledyne Scientific and Imaging for providing implant isolation for the device fabrication, DiVA pulsed IV measurements, and facilitating the 30 GHz OIP3 measurements at Maury Microwave Corporation. The authors thank Prof. James F. Buckwalter (UCSB) for helpful discussions.

This work was supported by the Defense Advanced Research Projects Agency DREaM program (DARPA, Dr. Young-Kai Chen and Dr. Daniel Green) and the Office of Naval Research (ONR, Dr. Paul Maki). This work also utilized in part the UCSB HFM lab which has been supported by multiple USA DoD DURIP grants through the ONR (Dr. Paul Maki) and the Army Research Office (ARO, Dr. James Harvey).

## References

[1] U. K. Mishra and M. Guidry, "Lateral GaN Devices for Power Applications (from kHz to GHz)," in *Power GaN Devices: Materials, Applications and Reliability*, M. Meneghini, G. Meneghesso, and E. Zanoni, Eds. Cham: Springer International Publishing, 2017, pp. 69–99.

[2] M. Micovic, D. Brown, D. Regan, J. Wong, J. Tai, A. Kurdoghlian, F. Herrault, Y. Tang, S. D. Burnham, H. Fung, A. Schmitz, I. Khalaf, D. Santos, E. Prophet, H. Bracamontes, C. Mcguire, and R. Grabar, "Ka-band LNA MMICs realized in fmax > 580 GHz GaN HEMT Technology," *2016 IEEE Compd. Semicond. Integr. Circuit Symp.*, pp. 1–4, 2016.

[3] R. S. Howell, E. J. Stewart, R. Freitag, J. Parke, B. Nechay, M. King, S. Gupta, M. Snook, I. Wathuthanthri, P. Ralston, and H. G. Henry, "Advances in the Super-Lattice Castellated Field Effect Transistor (SLCFET) for wideband low loss RF switching applications," in *2016 IEEE MTT-S International Microwave Symposium (IMS)*, 2016, pp. 1–3.

[4] B. Romanczyk, S. Wienecke, M. Guidry, H. Li, E. Ahmadi, X. Zheng, S. Keller, and U. K. Mishra, "Demonstration of Constant 8 W/mm Power Density at 10, 30, and 94 GHz in State-of-the-Art Millimeter-Wave N-Polar GaN MISHEMTs," *IEEE Trans. Electron Devices*, vol. 65, no. 1, pp. 45–50, Jan. 2018.

[5] M. H. Wong, S. Keller, N. S. Dasgupta, D. J. Denninghoff, S. Kolluri, D. F. Brown, J. Lu, N. A. Fichtenbaum, E. Ahmadi, U. Singisetti, A. Chini, S. Rajan, S. P. DenBaars, J. S. Speck, and U. K. Mishra, "N-polar GaN epitaxy and high electron mobility transistors," *Semicond. Sci. Technol.*, vol. 28, no. 7, p. 074009, Jul. 2013.

[6] S. A. Maas, *Nonlinear Microwave and RF Circuits*, 2nd ed. Artech House, 2003.

[7] A. Arias, P. Rowell, J. Bergman, M. Urteaga, K. Shinohara, X. Zheng, H. Li, B. Romanczyk, M. Guidry, S. Wienecke, E. Ahmadi, S. Keller, and U. Mishra, "High performance N-polar GaN HEMTs with OIP3/Pdc ~12dB at 10GHz," in *2017 IEEE Compound Semiconductor Integrated Circuit Symposium (CSICS)*, 2017, pp. 1–3.

[8] A. Arias, P. Rowell, J. Bergman, M. Urteaga, K. Shinohara, X. Zheng, H. Li, B. Romanczyk, M. Guidry, S. Wienecke, E. Ahmadi, S. Keller, and U. Mishra, "N-polar GaN HEMTs with State-of-the-Art Linearity Performance (OIP3/PDC) at 10 and 30 GHz," *GOMAC Tech*, pp. 1–4, 2018.

[9] B. Romanczyk, H. Li, M. Guidry, E. Ahmadi, S. Wienecke, X. Zheng, S. Keller, and U. K. Mishra, "Record 30 GHz Power Performance of mm-Wave N-Polar GaN Deep Recess MISHEMTs with 59.7% PAE and 4.73 W/mm," in *GOMAC Tech*, 2018.

[10] S. Wienecke, B. Romanczyk, M. Guidry, H. Li, E. Ahmadi, K. Hestroffer, X. Zheng, S. Keller, and U. K. Mishra, "N-Polar GaN Cap MISHEMT With Record Power Density Exceeding 6.5 W/mm at 94 GHz," *IEEE Electron Device Lett.*, vol. 38, no. 3, pp. 359–362, Mar. 2017.

[11] E. Ahmadi, S. Keller, and U. K. Mishra, "Model to explain the behavior of 2DEG mobility with respect to charge density in N-polar and Ga-polar AlGaN-GaN heterostructures," *J. Appl. Phys.*, vol. 120, no. 11, p. 115302, Sep. 2016.

[12] T. Gasseling, E. Gatard, C. Charbonniaud, and A. Xiong, "Assets of source pull for NVNA based load pull measurements," in *79th ARFTG Microwave Measurement Conference*, 2012, pp. 1–5.

[13] "Datasheet 4T-097: MT1000 and MT2000 – Mixed-Signal Active Load Pull System (1.0 MHz to 40.0 GHz) And MT2001 System Software." [Online]. Available: https://www.maurymw.com/pdf/datasheets/4T-097.pdf. [Accessed: 02-Jan-2019].

[14] S. A. Maas and A. Crosmun, "Modeling the gate I/V characteristic of a GaAs MESFET for Volterra-series analysis," *IEEE Trans. Microw. Theory Tech.*, vol. 37, no. 7, pp. 1134–1136, Jul. 1989.

[15] T. Palacios, S. Rajan, A. Chakraborty, S. Heikman, S. Keller, S. P. DenBaars, and U. K. Mishra, "Influence of the Dynamic Access Resistance in the gm and ft Linearity of AlGaN/GaN HEMTs," *IEEE Trans. Electron Devices*, vol. 52, no. 10, pp. 2117–2123, Oct. 2005.

[16] I. Angelov, M. Thorsell, K. Andersson, N. Rorsman, E. Kuwata, H. Ohtsuka, and K. Yamanaka, "On the large-signal modeling of High Power AlGaN/GaN HEMTs," in *2012 IEEE/MTT-S International Microwave Symposium Digest*, 2012, pp. 1–3.

[17] P. M. Cabral, J. C. Pedro, and N. B. Carvalho, "Nonlinear Device Model of Microwave Power GaN HEMTs for High Power-Amplifier Design," *IEEE Trans. Microw. Theory Tech.*, vol. 52, no. 11, pp. 2585–2592, Nov. 2004.